Vibrationally assisted below-threshold ionization

Spencer L. Horton,[1] Yusong Liu,[1] Pratip Chakraborty,[2] Spiridoula Matsika,[2] and Thomas Weinacht[1]

[1]*Department of Physics and Astronomy, Stony Brook University, Stony Brook, New York 11794, USA*

[2]*Department of Chemistry, Temple University, Philadelphia, Pennsylvania 19122, USA*

We perform time-resolved UV pump (4.77 eV) and VUV probe (7.94 eV) measurements of internal conversion of 1,3-cyclohexadiene (CHD). Our measurements reveal a substantial ionization of the "hot" ground state following internal conversion despite the fact that our probe photon energy is below the ionization potential (8.21 eV). With the aid of electronic structure calculations, we interpret our results in terms of vibrationally assisted below-threshold ionization, where vibrational energy is converted to electronic energy. The effect relies on both having vibrational modes which allow for this vibrational-electronic coupling and exciting these modes during the internal conversion. We contrast our measurements in CHD with another similar molecule, *cis,cis*-1,3-cyclooctadiene (*cis,cis*-COD), for which we do not see the effect.

I. INTRODUCTION AND MOTIVATION

The conversion of electronic potential energy into nuclear kinetic energy is one of the most ubiquitous features of photoexcited molecular dynamics. As a wave packet moves down an excited potential energy surface following photoabsorption, electronic potential energy is converted into nuclear kinetic energy. In a diatomic molecule, kinetic and potential energy are exchanged every half period for motion in a bound state. This exchange can be observed in many time-resolved spectroscopies [1,2]. However, in larger polyatomic systems with many degrees of vibrational freedom, the exchange of nuclear kinetic energy into electronic potential energy is much harder to observe because the nuclear kinetic energy is distributed over many modes.

Our recent development of a ultraviolet (UV) (260 nm, 4.77 eV) and vacuum-ultraviolet (VUV) (156 nm, 7.94 eV) time-resolved pump-probe photoionization apparatus allows us to study this conversion of vibrational kinetic energy into electronic energy via vibrationally assisted below-threshold ionization. We consider the ionization of 1,3-cyclohexadiene (CHD), whose ionization potential is slightly above our photon energy of 7.94 eV. The excited-state dynamics of CHD been the subject of intense study [3–7], and its neutral excited-state dynamics are well understood. Initial excitation to the first bright state (S_1) is followed by rapid internal conversion to the ground state, with some fraction of the molecules isomerizing to form 1,3,5-hexatriene (HT). It is well established that there are no traps on the excited state, and after about 200 fs there is no longer any probability of finding the molecule in an excited state. Thus, with an ionization potential (IP) of 8.21 eV,[1] it is a prime candidate to explore vibrationally assisted below-threshold ionization. After excitation and internal conversion, there is about 5 eV of energy in the vibrationally hot ground state. If some of this

energy can be converted into electronic potential energy, then this would allow for below-threshold ionization.

We contrast our measurements in CHD with similar measurements for *cis,cis*-1,3-cyclooctadiene (*cis,cis*-COD), which has similar relaxation dynamics to CHD but a higher IP of 8.58 eV.

II. EXPERIMENTAL APPARATUS

We use a Ti:sapphire laser (1.2 mJ, 1 kHz, 30 fs, 780 nm) to generate ultrafast UV and VUV pulses. In conjunction with a time-of-flight mass spectrometer (TOFMS), we make use of these pulses to perform pump-probe ion yield measurements on CHD and *cis,cis*-COD. Gas-phase CHD and *cis,cis*-COD molecules are injected into the vacuum chamber as an effusive molecular beam.

The IR beam from the amplifier is split into two portions which have pulse energies of 1.1 mJ and 100 μJ. The 1.1 mJ of IR is used to create 50 μJ of UV ($\hbar\omega = 4.77$ eV) light through second-harmonic generation (SHG) followed by third-harmonic generation (THG) in beta barium borate (BBO) crystals with a calcite delay compensator. An uncoated 1-mm-thick CaF$_2$ window is inserted into the beam at 45° to act as a beam splitter for the UV. The 5-μJ pulse from the front surface reflection of the CaF$_2$ window is used as the UV pump in our experiments. The back surface reflection leads to a second pump pulse about 2 ps after the main one, but as this second pulse is horizontally displaced relative to the first pulse from the front surface reflection, we can attenuate it substantially with the use of an iris. Approximately 100 nJ of fifth-harmonic (VUV) probe-pulse ($\lambda = 156$ nm, $\hbar\omega = 7.94$ eV) is generated by focusing the remaining 40 μJ of UV and 100 μJ of IR into an argon gas cell utilizing a noncollinear four-wave-mixing process [8–10]. This mechanism takes advantage of phase matching at a relatively high pressure (330 Torr) of argon gas, which increases the conversion efficiency.

The VUV pulse passes through a 500-μm-thick CaF$_2$ window into an interaction chamber, which is maintained at a pressure of 5×10^{-7} Torr. The unfocused VUV pulse first passes under the repeller plates of our TOFMS. It is then reflected by a dichroic mirror of radius of curvature $R = 268$ mm. The mirror has a high reflectivity coating of $>90\%$ at 0° for 156- to

---

[1]The IPs used in this paper are all calculated at the EOM-IP-CCSD/6-311+G(d) level using Q-CHEM. The calculated and experimentally measured values are listed in Table I. We do not have measured IPs for all reactants and products, so we use the calculated values for consistency.
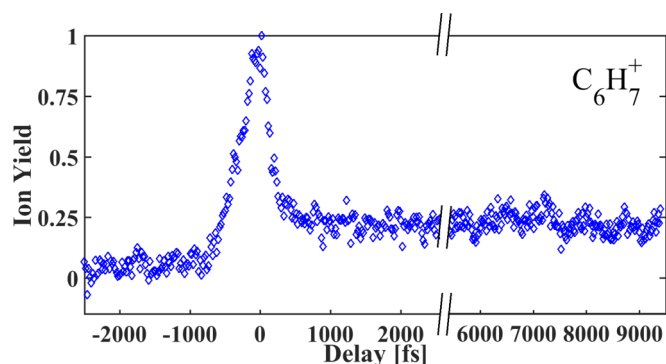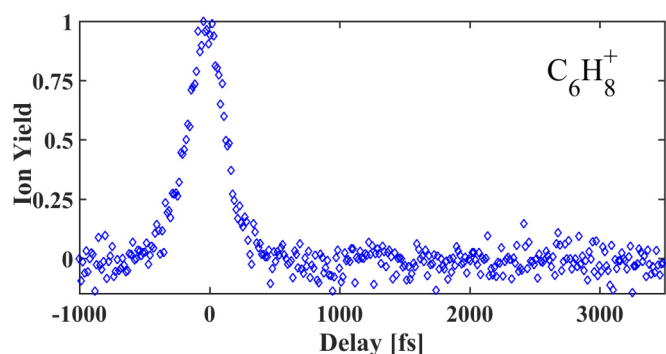
FIG. 1. CHD pump probe data for $C_6H_7^+$ fragment.

160-nm light and $<10\%$ reflectivity for 260 and 800 nm. This enables the residual UV and IR radiation left over from VUV generation to be separated from the VUV. The reflected VUV pulse is then focused under the TOFMS repeller plates. The 5 μJ of UV reserved for the pump is sent through the dichroic mirror and also focused under the TOFMS repeller plates. More details about the apparatus can be found in Ref. [11].

III. COMPUTATIONAL METHODS

Conical intersections (CIs) between S_0 and S_1 were calculated for *cis,cis*-COD using the state averaged complete active space self-consistent field (SA-CASSCF) method and the cc-pVDZ basis set. An active space of four electrons in four orbitals (4,4) was used and two states were averaged (SA2-CASSCF). Linear interpolations in internal coordinates at the SA4-CASSCF level were used to connect *cis,cis*-COD to the two CIs found and the CIs to the products. The conical intersection for CHD is taken from previous work [7]. Linear interpolations between CHD and the CI and between HT and the CI were computed using CASSCF (6,6) with the cc-pVDZ basis set and averaging three states. The computational packages GAUSSIAN [12] and COLUMBUS [13] were used for the CASSCF calculations.

For the Franck-Condon (FC) factor calculations, S_0 and the D_0 were optimized at the B3LYP/6-31G(d) and UB3LYP/6-31G(d) levels, respectively, for both molecules. We define the FC factors as $|\langle \psi_{v_{\text{final}}} | \psi_{v_{\text{initial}}} \rangle|^2$, where $\psi_{v_{\text{initial}}}$ and $\psi_{v_{\text{final}}}$ are the initial and final vibrational states. Frequency calculations were performed at the same level of theory in order to obtain the normal modes. FC factors between S_0 and D_0 for all the

molecules were calculated using ezSpectrum 3.0 code [14]. ezSpectrum 3.0 can calculate the FC factors between the initial and target vibrational state wave functions using two approximations: parallel normal modes approximation and Duschinsky rotations of the normal modes as full-dimensional integrals. We have used the latter method to do the calculations. The S_0 and D_0 minima for a molecule were used as initial and target electronic states, respectively. As we were interested to see ionization from the hot vibrational levels of S_0 to the lowest lying vibrational levels of D_0, the energy threshold for S_0 was kept at 4.20 eV, while that for D_0 was kept at 0.60 eV. The maximum vibrational excitations in the initial state and the target state were taken as 5 and 2 respectively in order to keep the calculations tractable. The spectrum intensity threshold was set at 10^{-7}. The optimizations and frequency calculations were performed using Q-CHEM software [15],

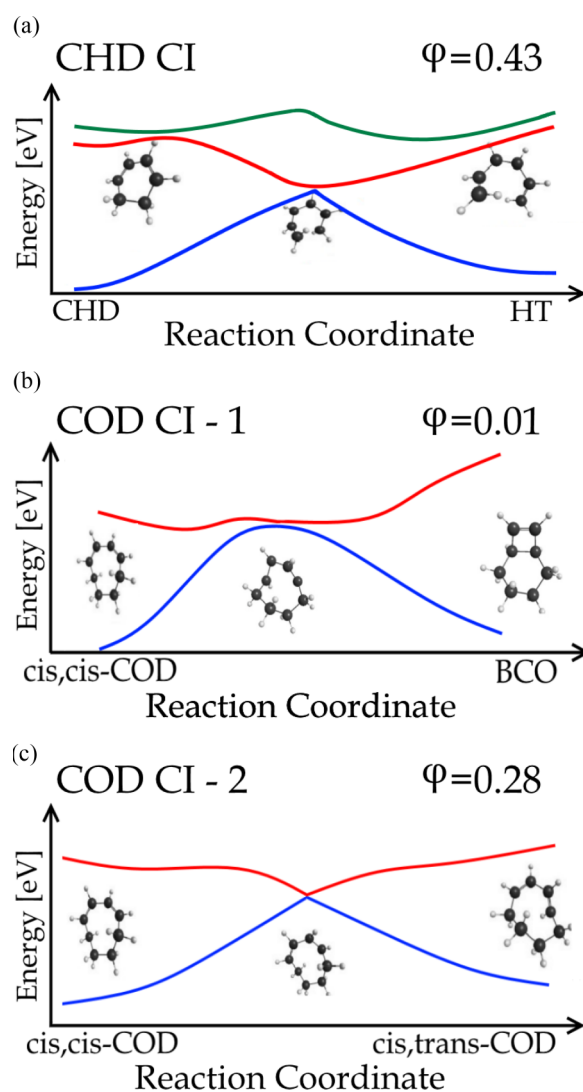FIG. 2. *cis,cis*-COD pump probe data for $C_6H_8^+$ fragment.

FIG. 3. Potential energy surfaces (PES) and relevant CIs for (a) CHD that can lead to isomerization into HT, (b) *cis,cis*-COD that can lead to isomerization to BCO, and (c) *cis,cis*-COD that can lead to isomerization to *cis,trans*-COD, where ϕ indicates the quantum yield of the photochemical products [4,18]. Blue [bottom curve] $\Rightarrow S_0$, red [middle curve in panel (a) and top curve in panels (b) and (c)] $\Rightarrow S_1$, and green [top curve in panel (a)] $\Rightarrow S_2$.

TABLE I. Calculated vertical IPs, adiabatic IPs, and the average measured IPs for CHD, *cis,cis*-COD and their relevant isomers

Molecule	Calculated vertical IP [eV]	Calculated adiabatic IP [eV]	Measured IP [eV]
1,3-Cyclohexadiene (CHD)	8.21	8.04	8.26 [17,20–25]
1,3,5-Hexatriene (HT)	8.37	8.12	8.31 [17,26–28]
cis,cis-1,3-cyclooctadiene (*cis,cis*-COD)	8.58	8.26	8.68 [23]
cis,trans-1,3-cyclooctadiene (*cis,trans*-COD)	8.42	7.98	N.A.
cis-bicyclo[4,2,0]oct-7ene (BCO)	9.13	8.87	N.A.

and MACMOLPLT [16] was used to visualize the molecules and normal modes. IPs for all systems were calculated at the EOM-IP-CCSD/6-311+G(d) level using Q-CHEM.

IV. EXPERIMENTAL RESULTS

UV-VUV pump-probe experiments were performed on CHD, and the results for fragment $C_6H_7^+$ can be seen in Fig. 1. In the UV-VUV pump-probe measurements we conducted, the most prominent signal is from the parent ion ($C_6H_8^+$). However, since the parent ion can be formed by two-photon absorption from our pump pulse, there is substantial background on the pump-probe signal. Therefore, we focus our attention on the

$C_6H_7^+$ fragment, which is background free, but can still be formed by single-photon absorption from each of the pump and probe pulses. The appearance energies (AEs) of the fragments in CHD are taken from Ref. [17]. The total energy available from absorption of both UV and VUV pulses is 12.7 eV, so energetically it is possible to form the parent ion, $C_6H_8^+$, as well as $C_6H_7^+$ (AE is 10.82 eV).

Figure 1 shows the $C_6H_7^+$ yield as a function of pump-probe delay. We focus our attention on the difference in ion yield between positive and negative delays. At negative time delays, the VUV pulse precedes the UV pulse, and vice versa for positive time delays. Our pump-probe data shows a cooperative UV-VUV pump-probe signal in $C_6H_7^+$ at time zero. After time
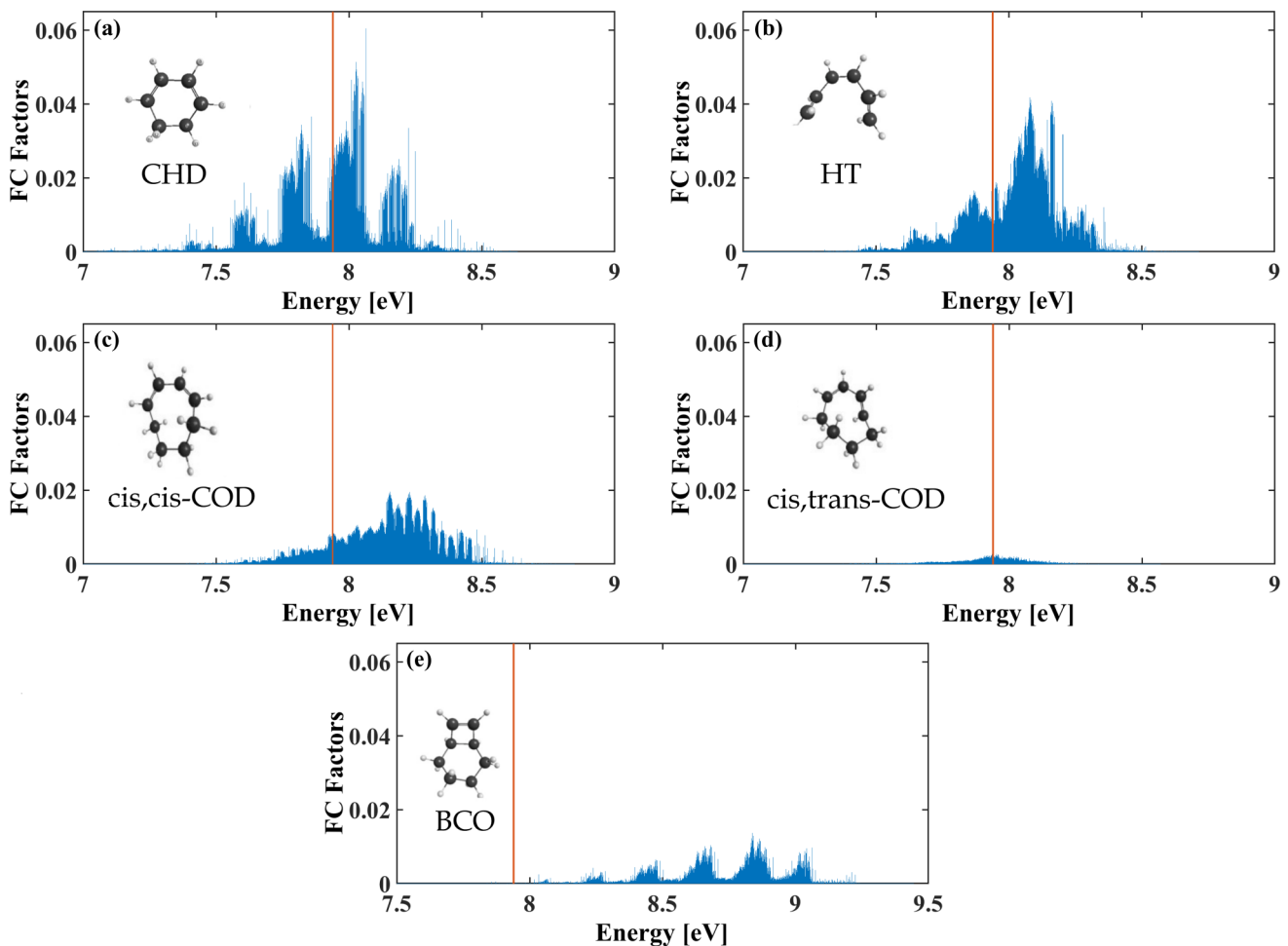

FIG. 4. Franck-Condon factors (FCF) for vibrational levels in (a) CHD, (b) HT, (c) *cis,cis*-COD, (d) *cis,trans*-COD, and (d) BCO between their ground states, S_0, and first ionic states, D_0. The red (vertical) line in each of the subplots indicates the probe photon energy.

zero, when the UV pulse has been incident on the molecule and it has undergone internal conversion down to the ground state (where the ionization potential of both isomers is above the photon energy of our probe), we still measure a yield which is about 20% of the yield in ionizing from the excited state (for which the probe is well above the ionization potential) near zero time delay.

For comparison, UV-VUV pump-probe experiments were also performed on a similar molecule, *cis,cis*-COD. The AEs of *cis,cis*-COD are not available, but binning over all possible fragments in the TOFMS we see a pump-probe signal for the parent, $C_8H_{12}^+$, and the fragments $C_7H_9^+$, $C_6H_8^+$, and $C_5H_7^+$. In contrast to CHD, none of the resulting products from the UV-VUV pump-probe scan show any sign of a ledge (below-threshold ionization) after time zero. The fragment $C_6H_8^+$ has the most prominent signal, and the results of the pump-probe measurements can be seen in Fig. 2.

V. CALCULATIONS

In order to interpret the persistence of a nonzero ionization yield for CHD at long positive time delays, we consider the excited-state dynamics in more detail and perform a number of calculations. As noted above, CHD is a well-studied molecule, and its relaxation dynamics after UV pumping have been considered in detail [3–7]. The UV pump pulse launches a wave packet on the bright S_1 state (see Fig. 5), which quickly changes character diabatically because of an avoided crossing with the dark S_2 state.

From the S_1 state, two CIs have been identified between S_1 and S_0, with one being symmetric and the other asymmetric. According to Ref. [6], the asymmetric CI dominates the relaxation dynamics. Figure 3(a) shows a diagram of the CI between the S_1 and S_0 states in CHD. Once on S_0 again, the molecule can go back to ground-state CHD or isomerize into 1,3,5-hexatriene (HT). The branching ratio for forming ground-state CHD versus HT has been measured to be 7:3 [4] (represented in the figure as the quantum yield ϕ).

The excited-state dynamics for *cis,cis*-COD after being pumped in the UV have also been studied. UV-IR femtosecond pump-probe measurements have been performed on COD by Fuss *et al.* in Ref. [18], and nanosecond UV laser irradiation of *cis,cis*-COD was performed in Ref. [19]. We performed electronic structure calculations on *cis,cis*-COD and identified two possible CIs that can lead to internal conversion back into its ground state, isomerization into *cis*-bicyclo[4,2,0]oct-7ene (BCO) or isomerization to *cis,trans*-1,3-cyclooctadiene (*cis,trans*-COD). *cis,cis*-COD and *cis,trans*-COD have several conformers. In this work, we used the lowest energy conformer in each case, which has a population of 70% and 99%, for *cis,cis*-COD and *cis,trans*-COD, respectively. In Figs. 3(b) and 3(c), we identify the reaction pathways for the different CIs, the geometry of the molecule at the CIs, and the relative quantum yields to the different photochemical products, ϕ [18]. For *cis,cis*-COD, as in CHD, we have similar neutral-state dynamics that lead to ultrafast internal conversion and isomerization after excitation with the UV pump.

In Table I, we list our calculated vertical IPs, calculated adiabatic IPs, and the average of measured values for the IPs of all the relevant isomers. From Table I, one can see that
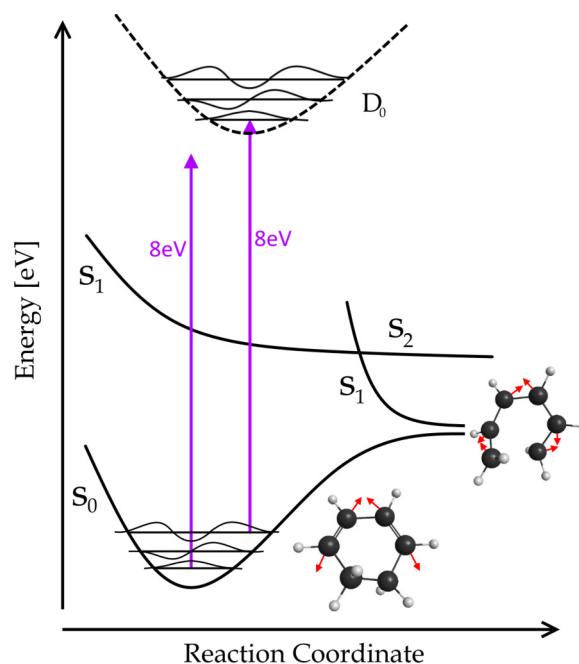

FIG. 5. In S_0 and D_0, we sketch vibrational levels and wave functions to illustrate the Franck-Condon principle that can lead to below-threshold ionization. This CHD energy level cartoon illustrates the FC overlap argument for vibrationally assisted ionization. At the conical intersection between S_0 and S_1 is a picture of the molecule with the motion of the carbons along the derivative coupling vector indicated. Next to S_0 is a picture indicating the normal mode motion associated with the coordinate for which the high lying vibrational levels in S_0 have good FC overlap with low-lying vibrational levels in D_0.

our calculated vertical transition IPs are within 0.1 eV of the measured values. All of the vertical IPs of the possible products are at least 0.26 eV or more above our probe photon energy. This indicates that our signal in CHD at long times is not simply due to formation of an isomer with an ionization potential lower than our probe photon energy.
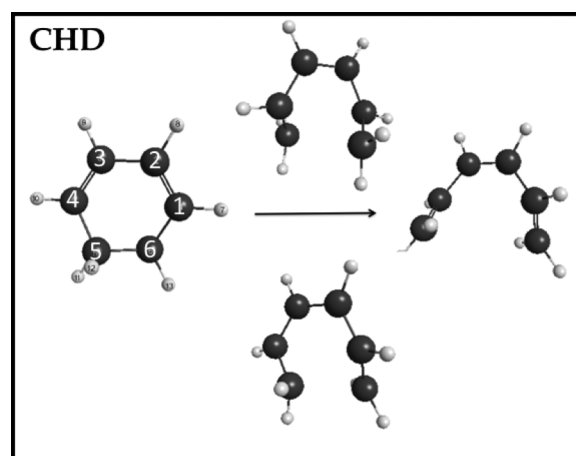

FIG. 6. CHD geometry at the S_0 minimum (left), the asymmetric CI (top), symmetric CI (bottom), and after isomerization into HT (right).

TABLE II. Calculated C-C bond movement for CHD.

	1–2 [Å]	2–3' [Å]	3–4' [Å]	4–5' [Å]	1–6' [Å]	React (5–6) [Å]	rms D [Å]
CHD	1.35	1.46	1.35	1.51	1.51	1.53	
Asymmetric CI	1.43	1.41	1.38	1.448	1.44	2.19	
Symmetric CI	1.44	1.38	1.44	1.49	1.49	2.72	
HT	1.47	1.35	1.47	1.34	1.34	3.35	
			Difference of bonds lengths from CHD				
Asymmetric CI	0.08	−0.05	0.03	−0.06	−0.07	0.66	0.68
Symmetric CI	0.09	−0.08	0.09	−0.02	−0.02	1.19	1.20
HT	0.12	−0.11	0.12	−0.17	−0.17	1.83	1.85

Finally, in order to understand how ground-state vibrations can lead to below-threshold ionization, we look at the FC factors between excited vibrational levels in the ground state, S_0, and lower lying vibrations in the ground state of the cation, D_0. Our aim is to identify high-lying vibrational levels in S_0 that have a good FC overlap with low-lying vibrational levels in D_0 that can be ionized with 7.94 eV of photon energy.

Figure 4 shows the calculated FC factors for CHD, HT, *cis-cis*-COD, *cis,trans*-COD, and BCO. We used the calculated adiabatic IP in each case. The *x* axis is the energy difference between the vibrational levels in S_0 and D_0. The *y* axis is the FC factors for the different vibrational levels. The VUV photon energy is indicated by a red (vertical) line in all the subplots in Fig. 4.

Figure 4(a) shows the FC factors between vibrational levels in the ground state, S_0, and the first ionic state, D_0, for CHD. We note that a significant fraction of the vibrational levels in the hot S_0 can be ionized to D_0 with our probe pulse—those to the left of the red line. This is also true for HT, but in contrast, we note that a smaller fraction of vibrational levels can be ionized for *cis,cis*-COD, *cis,trans*-COD, and BCO. The magnitudes of the FC factors are also much smaller in *cis,cis*-COD, *cis,trans*-COD, and BCO.

VI. DISCUSSION

The fact that the bulk of the FC factors lie to the right of the red line in Fig. 4 for *cis,cis*-COD, *cis,trans*-COD, and BCO, in addition to the fact that they are much smaller than for CHD or HT, is consistent with our measurements of hot ground-state ionization for CHD, but no hot ground-state ionization for COD.

The FC factors in Fig. 4(a) have a regular structure with a period of ∼0.2 eV, corresponding to the frequency of C-C stretching. This suggests that if C-C stretching motion is activated during internal conversion, then it can lead to the vibrationally assisted below-threshold ionization. We therefore considered whether the passage of the molecule through the relevant CI during internal conversion could

excite this motion. Figure 5 shows the normal mode, which is mainly responsible for the vibrational progression seen in the FC factors for CHD. This mode involves the symmetric stretching of both double bonds in the molecule. The figure also shows the derivative coupling vector at the conical intersection between S_1 and S_0. The motion indicated by this vector is also mainly along the stretching motion of the C-C bonds, and it will be activated as the wave packet passes through the CI. The similarity between the coupling vector and the normal mode indicates that much of the electronic energy converted to vibrational energy after passing through the CI will be excitation along the normal mode shown. Another indication of the vibrational excitation along the C-C modes is given by calculating the rms deviation of the six C-C bonds in CHD between the FC region and the CI.

In Appendix A, we calculate the C-C bond lengths at the S_0 minimum, the symmetric CI, the asymmetric CI, and HT geometries. The rms displacement of the carbons at the asymmetric CI from their initial S_0 minimum geometry is 0.7 Å, indicating that there is indeed substantial C-C stretching activated during passage through the CI. We also calculated the bond lengths for S_0 and the D_0. Going from S_0 to D_0, the double bonds expand while the single bonds compress, and this is reflected in the progression seen in the FC factors associated with vibrational mode 27, shown in Fig. 5, at 1660 cm^{-1} (0.2 eV; see Appendix B for vibrational modes of CHD).

In *cis,cis*-COD, *cis,trans*-COD, and BCO, the FC factors at 7.94 eV are just too small to see significant below-threshold ionization.

Before concluding, another possibility that we consider in order to interpret our results is excitation of vibrationally hot CHD into a neutral Rydberg state by the probe, from which the molecule can autoionize as a result of the excess vibrational energy. The absorption spectrum of CHD can be found in Refs. [29–31], and there is a strong absorption band at 7.94 eV. The question then is whether absorption to such a high excited neutral state can lead to autoionization. In order to address this question, we looked at the character of the states that lead to the strong absorption at 7.94 eV and

TABLE III. Calculated bond lengths for S_0 and D_0 for CHD.

	1–2 [Å]	2–3' [Å]	3–4' [Å]	4–5' [Å]	1–6' [Å]	React (5–6) [Å]
CHD D_0	1.39	1.42	1.39	1.48	1.48	1.54
CHD S_0	1.35	1.46	1.35	1.51	1.51	1.53
D_0-S_0	0.04	−0.05	0.04	−0.03	−0.03	0.01

TABLE IV. Vibrational modes of CHD.

Vibrational mode number	Frequency [cm^{-1}]	Vibrational mode number	Frequency [cm^{-1}]
1	191	19	1214
2	302	20	1281
3	481	21	1370
4	520	22	1379
5	573	23	1419
6	675	24	1456
7	766	25	1500
8	782	26	1511
9	859	**27**	**1660**
10	940	28	1725
11	971	29	2981
12	973	30	2992
13	990	31	3076
14	1013	32	3076
15	1054	33	3166
16	1078	34	3173
17	1183	35	3188
18	1201	36	3197

considered the probability of ionization for states 0.1–0.3 eV below-threshold. In Ref. [32], it is indicated that autoionization of anthracene and naphthalene with 1–2 eV of vibrational energy only takes place for energies up to 0.1 eV below the ionization threshold. Furthermore, the character of the state in CHD which dominates the absorption at 7.94 eV is that of a valence state [$8\,^1A(V_3)$]. This would require internal conversion prior to autoionization, and the internal conversion would lead to lower electronic states, which are even less likely to autoionize. Therefore, we argue that the ionization yield that we measure for positive pump-probe delays is dominated by vibrationally assisted ionization rather than Rydberg excitation followed by autoionization.

VII. CONCLUSION

We observe below-threshold ionization of CHD, which we interpret in terms of vibrationally assisted ionization, where vibrational energy is converted to electronic energy. This is facilitated by the excitation of C-C stretching vibrations, which are activated during internal conversion from the photoexcited state down to the ground state.

APPENDIX A: CHD RELAXATION GEOMETRIES

Figure 6 shows the CHD geometries at the S_0 minimum, the asymmetric CI, symmetric CI, and after isomerization into HT. The carbons are labeled 1 through 6 in the S_0 geometry.

As the molecule goes through the symmetric and asymmetric CIs, the movement of the carbons is documented in Table II. The rms displacement of the carbons going through the asymmetric stretch is 0.68 Å, and the rms displacement of the carbons going through the symmetric stretch is 1.20 Å. If the molecule isomerizes into HT, the rms displacement of the carbons is 1.85 Å.

In Table III are the calculated bond lengths for S_0 and D_0. They show that when going from S_0 to D_0 the single bonds compress and the double bonds expand.

APPENDIX B: VIBRATIONAL MODES OF CHD

Table IV lists the vibrational modes in CHD. The geometry optimization and frequency calculations were done with B3LYP/6-31G(d). Mode 27, in Table IV, is the mode we have identified that is associated with the coordinate where high-lying vibrational levels in S_0 have good FC overlap with low-lying vibrational levels in D_0, and can lead to ionization with a 7.94-eV probe.

[1] M. Dantus, R. Bowman, and A. Zewail, Nature (London) **343**, 737 (1990).

[2] T. Baumert, M. Grosser, R. Thalweiser, and G. Gerber, Phys. Rev. Lett. **67**, 3753 (1991).

[3] W. Fuß, W. Schmid, and S. Trushin, J. Chem. Phys. **112**, 8347 (2000).

[4] S. Adachi, M. Sato, and T. Suzuki, J. Phys. Chem. Lett. **6**, 343 (2015).

[5] S. Deb and P. M. Weber, Annu. Rev. Phys. Chem. **62**, 19 (2011).

[6] M. Garavelli, C. Page, P. Celani, M. Olivucci, W. Schmid, S. Trushin, and W. Fuss, J. Phys. Chem. A **105**, 4458 (2001).

[7] M. Kotur, T. Weinacht, B. J. Pearson, and S. Matsika, J. Chem. Phys. **130**, 134311 (2009).

[8] M. Beutler, M. Ghotbi, F. Noack, and I. Hertel, Opt. Lett. **35**, 1491 (2010).

[9] M. Ghotbi, M. Beutler, and F. Noack, Opt. Lett. **35**, 3492 (2010).

[10] A. Börzsönyi, Z. Heiner, M. Kalashnikov, A. Kovács, and K. Osvay, Appl. Opt. **47**, 4856 (2008).

[11] S. L. Horton, Y. Liu, P. Chakraborty, S. Matsika, and T. Weinacht, J. Chem. Phys. **146**, 064306 (2017).

[12] M. J. Frisch, G. W. Trucks, H. B. Schlegel, G. E. Scuseria, M. A. Robb, J. R. Cheeseman, G. Scalmani, V. Barone, M. Bennucci, G. A. Petersson *et al.*, *Gaussian09 Revision E.01* (Gaussian Inc., Wallingford, CT, 2009).

[13] H. Lischka, T. Müller, P. G. Szalay, I. Shavitt, R. M. Pitzer, and R. Shepard, Wiley Interdiscip. Rev.: Comput. Mol. Sci. **1**, 191 (2011).

[14] V. Mozhayskiy and A. Krylov, EZSPECTRUM, http://iopenshell.usc.edu/downloads.

[15] Y. Shao, Z. Gan, E. Epifanovsky, A. Gilbert, M. Wormit, J. Kussmann, A. Lange, A. Behn, J. Deng, X. Feng *et al.*, Mol. Phys. **113**, 184 (2015).

[16] B. M. Bode and M. S. Gordon, J. Mol. Graphics Modell. **16**, 133 (1998).

[17] J. L. Franklin and S. R. Carroll, J. Am. Chem. Soc. **91**, 6564 (1969).

[18] W. Fuß, S. Panja, W. E. Schmid, and S. A. Trushin, Mol. Phys. **104**, 1133 (2006).

[19] K. Komori-Orisaku, Y. Hirose, and I. Iwakura, *Photochemical Photobiological Sciences* (Royal Society of Chemistry, 2017).

[20] K. Kimura, *Handbook of HeI Photoelectron Spectra of Fundamental Organic Molecules* (Japan Scientific Societies Press, Tokyo, 1981).

[21] G. Bieri, F. Burger, E. Heilbronner, and J. P. Maier, Helv. Chim. Acta **60**, 2213 (1977).

[22] D. Demeo and M. El-Sayed, J. Chem. Phys. **52**, 2622 (1970).

[23] P. Bischof and E. Heilbronner, Helv. Chim. Acta **53**, 1677 (1970).

[24] S. Worley, T. Webb, D. H. Gibson, and T.-S. Ong, J. Organomet. Chem. **168**, C16 (1979).

[25] E. Heilbronner, T. Hoshi, J. L. von Rosenberg, and K. Hafner, Nouv. J. Chim. **1**, 105 (1976).

[26] M. Allan, J. Dannacher, and J. P. Maier, J. Chem. Phys. **73**, 3114 (1980).

[27] R. Gavin, Jr. and S. A. Rice, J. Chem. Phys. **60**, 3231 (1974).

[28] W. Price and A. Walsh, Proc. Royal Soc. London, Ser. A **185**, 182 (1946).

[29] R. P. Frueholz, W. M. Flicker, O. A. Mosher, and A. Kuppermann, J. Chem. Phys. **70**, 2003 (1979).

[30] R. McDiarmid, A. Sabljić, and J. Doering, J. Chem. Phys. **83**, 2147 (1985).

[31] M. Merchán, L. Serrano-Andrés, L. S. Slater, B. O. Roos, R. McDiarmid, and X. Xing, J. Phys. Chem. A **103**, 5468 (1999).

[32] P. M. Johnson and T. J. Sears, J. Chem. Phys. **143**, 044305 (2015).